Neuron, Vol. 15, 159–168, July, 1995, Copyright © 1995 by Cell Press

Mapping Miniature Synaptic Currents to Single Synapses Using Calcium Imaging Reveals Heterogeneity in Postsynaptic Output

Timothy H. Murphy,*‡§ Jay M. Baraban,* and W. Gil Wier†
*Department of Neuroscience
Johns Hopkins University School of Medicine
Baltimore, Maryland 21205
†Department of Physiology
University of Maryland School of Medicine
Baltimore, Maryland 21201
‡Kinsmen Laboratory
Department of Psychiatry
University of British Columbia
Vancouver, British Columbia V6T 1Z3
Canada

Summary

The amplitudes and kinetics of miniature excitatory synaptic currents (MESCs) in mammalian central neurons vary widely. It is unclear whether this variability occurs at each synapse or arises from differences among a heterogeneous population of synapses. Furthermore, it is not known how variability in these currents would affect their associated postsynaptic Ca^{2+} transients. To address these questions, we conducted simultaneous Ca^{2+} imaging and patch-clamp recordings from cultured cortical neurons and mapped individual MESCs to identified synapses displaying coincident dendritic miniature synaptic Ca^{2+} transients (MSCTs). Measurements of MSCTs at dendritic sites that displayed multiple events revealed that MSCT amplitude varied considerably at each site. Simultaneous measurement of MESCs and MSCTs at these sites indicated that variability in coincident synaptic currents contributes to the differences in Ca^{2+} transient amplitude. The ability of single synapses to exhibit variable output may enable them to engage intracellular signaling pathways at different levels of intracellular Ca^{2+}.

Introduction

The synapses on neurons of the central nervous system are structurally and functionally diverse. Thousands of different synaptic contacts are present on these cells, which have highly branched and morphologically varied dendritic arbors (Amaral et al., 1990). The amplitudes and kinetics of the spontaneous miniature excitatory synaptic currents (MESCs) arising at these contacts vary widely (reviewed in Lisman and Harris, 1993; Stevens, 1993). Although this variability is well documented in records of activity made from the cell soma, its origin can potentially be attributed to a number of different factors, which include differences in postsynaptic receptor responsiveness between synapses, variation in the number of transmitter quanta released at a single synapse, and electrotonic filtering of measured currents. To distinguish among these possibilities and to understand how synaptic currents and Ca^{2+} transients are related in dendritic compartments, we have performed Ca^{2+} imaging and voltage-clamp recording simultaneously in cultured cortical neurons to detect both synaptic current and Ca^{2+} transient responses from single identified synapses.

Previous studies have described postsynaptic Ca^{2+} transients associated with evoked synaptic transmission (Regehr and Tank, 1990, 1992; Muller and Connor, 1991; Murphy et al., 1992; Alford et al., 1993; Perkel et al., 1993; Malinow et al., 1994; reviewed in Regehr and Tank, 1994). These transients have a component attributed to the entry of Ca^{2+} through N-methyl-D-aspartate (NMDA)–type glutamate receptors (but see Miyakawa et al., 1992; Markram and Sakmann, 1994). Although these studies have been useful in defining the mechanisms by which Ca^{2+} enters the dendrite, it was not always possible to measure the effect of activity at just a single synapse. In contrast, by imaging dendritic intracellular Ca^{2+} concentration ($[Ca^{2+}]_i$) under conditions that allow only miniature release of transmitter and favor the activation of NMDA receptors (the absence of extracellular Mg^{2+}), we have recently recorded highly localized $[Ca^{2+}]_i$ transients, termed miniature synaptic Ca^{2+} transients (MSCTs; Murphy et al., 1994a). These transients were found to arise at discrete 1–2 μm^2 foci, consistent with the activation of single synapses. As these Ca^{2+} transients were blocked by NMDA-type glutamate receptor antagonists, we proposed that they arose via Ca^{2+} influx through these receptors during MESCs. Although the Ca^{2+} current associated with a single NMDA receptor–mediated MESC is less than 1 pA, $[Ca^{2+}]_i$ is expected to reach micromolar levels in the small volume of a dendritic process or spine, facilitating the detection of Ca^{2+} entry attributed to a single MESC (Zador et al., 1990; Koch and Zador, 1993).

MSCTs fit many of the anatomical, kinetic, and pharmacological criteria expected for postsynaptic Ca^{2+} transients triggered by the NMDA receptor component of MESCs. However, in our previous study (Murphy et al., 1994a), we did not directly determine how the two were related. To evaluate the relationship between MSCTs and MESCs, we have, in the present study, combined Ca^{2+} imaging (at a higher sampling rate of 30 Hz) with patch-clamp recording to correlate MESCs recorded at the cell soma with the appearance of MSCTs imaged in dendritic processes. This approach has allowed us to demonstrate that, as expected, MESCs trigger MSCTs; to establish that these unitary postsynaptic responses, attributed to NMDA receptors, vary within single synapses; and to investigate the relationship between synaptic currents and the resulting rise in dendritic $[Ca^{2+}]_i$.

§Present address: Kinsmen Laboratory, Department of Psychiatry, University of British Columbia, 2255 Wesbrook Mall, Vancouver, British Columbia, V6T 1Z3 Canada.

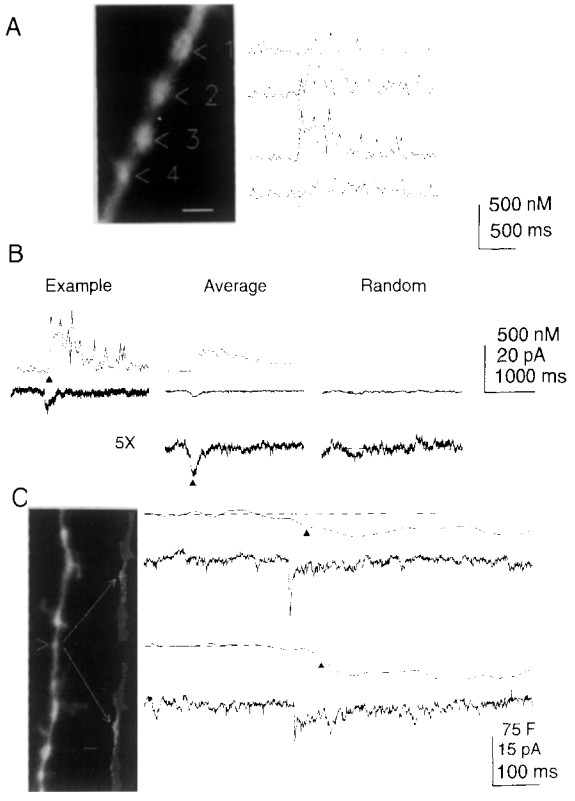

Figure 1. Simultaneous Records of Miniature Synaptic Currents and Ca^{2+} Transients from Identified Dendritic Sites

(A) High temporal resolution imaging is used to determine the time and site of MSCT initiation. Shown is a 360 nm excitation image of a Fura 2–filled dendrite from which four plots of $[Ca^{2+}]_i$ versus time were made at the adjacent sites. The site of MSCT initiation was defined by where the earliest rise in $[Ca^{2+}]_i$ was detected (site 3).

(B) (Left) An example of the temporal correlation between MESCs and MSCTs at site 3 (arrowhead marks the first rise in $[Ca^{2+}]_i$ above baseline for [B] and [C]). The $[Ca^{2+}]_i$ record shown above the current record is unfiltered and was collected at 30 Hz from a 1.0 μm^2 dendritic area. (Center) 19 records of MSCTs from 4 neurons were aligned by the first time point at which $[Ca^{2+}]_i$ rose above baseline and were then averaged (top trace). Current records corresponding to an interval 500 ms before to 2000 ms after this point (at arrow) were averaged and plotted beneath the record of average $[Ca^{2+}]_i$ ($n = 70$ current records from 12 neurons). A 5× scale is also shown for the averaged current (lowest trace); the calibration bar corresponds to the 1× records. (Right) An ensemble average current (from the same data sets) based on randomly aligned current records.

(C) Changes in raw Fura 2 fluorescence (380 nm excitation wavelength; thin traces on right) measured from the dendritic site (~2 μm^2) indicated by the single arrowhead (left) during two separate MSCTs (initiated at this site) and their correlation with MESCs (plotted below fluorescence). The initiation of each MSCT is shown in the respective gray-scale Ca^{2+} image indicated by the long arrows (left). These images were produced from the average of 3 consecutive video frames (100 ms), and the lightest gray value corresponds to the maximum $[Ca^{2+}]_i$ (250 nM). The raw fluorescence data traces are expressed in units of pixel value (F). Resting average pixel values over the dendrite were 123 (top record) and 127 (lower record), and resting background values were 33 and 32, respectively. Currents were recorded in the whole-cell mode. Data shown in (C) are from a different cell than that in (A) and (B).

Bars, 2 μm.

Results

A Temporal Correlation between MSCTs and MESCs

We have been able to localize the site and time at which MSCTs were first initiated on fine dendritic processes using video imaging of $[Ca^{2+}]_i$ with 33 ms temporal resolution and 0.15 μm spatial resolution (nominal pixel size) in the presence of tetrodotoxin (TTX) and no added Mg^{2+} (Figure 1). MSCT initiation sites were usually associated with morphological features of synaptic sites, such as a spine or a swelling (Figures 1A and 1C). These features were readily observed in averaged Fura 2 images produced at the Ca^{2+}-insensitive excitation wavelength (360 nm) of the dye, allowing the assessment of dendritic structure independently of changes in $[Ca^{2+}]_i$.

Measurement of synaptic currents in voltage-clamp recording mode (at −80 mV holding potential) indicated that the initiation of a MSCT was closely preceded by a MESC (Figure 1). For example, as shown in Figure 1B, a slow MESC, characteristic of NMDA receptor activation (Bekkers and Stevens, 1989; Hestrin, 1992; Carmignoto and Vicini, 1992), preceded the appearance of a Ca^{2+} transient at dendritic site 3 (Figure 1A). In another example (Figure 1C), MESCs that precede the first rise in $[Ca^{2+}]_i$ (raw fluorescence values are shown) have both fast and slow components that are presumably due to non-NMDA and NMDA-type glutamate receptors, respectively (Bekkers and Stevens, 1989; Silver et al., 1992). The temporal relationship between MSCTs and MESCs allowed us to assign synaptic currents to particular dendritic sites.

Since MESCs can occur at frequencies of 1–2 Hz in these cultured neurons and it is only possible to image a subset of the dendritic arbor (Murphy et al., 1994a), we wanted to check whether the apparent temporal correlation between MESCs and MSCTs was merely a chance coincidence. We assessed this possibility by averaging currents aligned by the first time point at which a rise in $[Ca^{2+}]_i$ was detected (Figure 1B, center; 1× and 5× gain shown). This ensemble average confirmed the temporal correlation between MESCs and MSCTs. In contrast, currents from the same data sets that were averaged using randomly generated intervals failed to yield a significant deviation from baseline (Figure 1B, right). As expected, the averaged currents were of lower amplitude than many of the single MESCs. The relatively low amplitude of the ensemble current average is likely due to the inability to align the current records precisely with those of $[Ca^{2+}]_i$, because of differences in the sampling rates used to obtain the two measurements. In addition, the noise present in the $[Ca^{2+}]_i$ measurements can obscure the precise detection of the MSCT upstroke, thereby affecting the alignment of the current records. In general, the latency between a MESC and the first rise in $[Ca^{2+}]_i$ during a MSCT ranged between 50 and 100 ms. Factors that contribute to this relatively long latency include the 33 ms time required to construct a video frame and the time required for Ca^{2+} to diffuse from the synapse (essentially a point source) into the 1 μm^2 area over which $[Ca^{2+}]_i$ was usually measured.

As a further test of the apparent correlation between

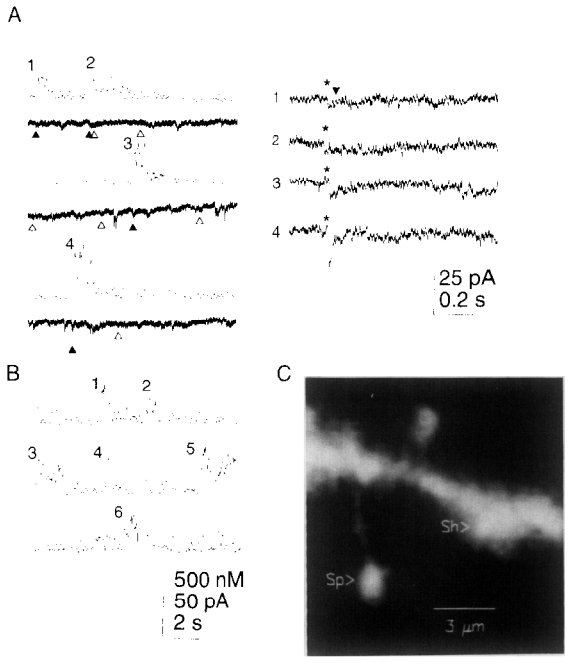

Figure 2. Examples of Variability in Synapse Output

(A) (Left) Repeated $[Ca^{2+}]_i$ transients (thin traces; filtered with a boxcar average of 3 points) were observed at a 1.0 μm^2 site on a dendritic shaft (see [C]) during three 10 s epochs, while synaptic currents were also measured (lower, thick traces). The small, closed arrowheads mark MESCs that are visible (above noise) at low time resolution and correlate with the initiation of MSCTs. (Right) MESCs shown at higher temporal and amplitude resolution aligned by the first point at which a rise in $[Ca^{2+}]_i$ was observed (arrowhead; determined from unfiltered data) for each of the 4 MSCT events. An asterisk indicates the presumed beginning of a MESC. The amplitudes of the synaptic currents were positively correlated with the MSCT amplitudes (R = 0.94; measured as in Figures 3A and 3B). Although the basal noise level of this recording is relatively high, this neuron exhibited a very low frequency of MESCs, allowing a more confident correlation between MESCs and MSCTs.

(B) During the same three 10 s epochs, 6 $[Ca^{2+}]_i$ transients were observed at a nearby spine. The open arrowheads below the current record in (A) (left) mark the time at which MSCTs were initiated at the spine site. In this example, synaptic currents associated with MSCTs that occured at the spine site were relatively smaller than those associated with activity at the shaft synapse.

(C) A 360 nm Fura 2 excitation image (Ca^{2+}-insensitive) indicating the dendritic shaft and spine site from which the data in (A) and (B), respectively, were obtained (Sp, spine; Sh, shaft). At both sites, resting $[Ca^{2+}]_i$ was less <75 nM on average.

MESCs and MSCTs, we measured the latency between the onset of each of the 8 MSCTs observed in the neuron from which the examples in Figures 1A and 1B were taken and the first negative current deflection that preceded each MSCT and exceeded 3 pA for a duration of 15 ms. The average latency between an inward current and the first rise in $[Ca^{2+}]_i$ was 91 ± 29 ms (mean ± SD). In contrast, when the time point of MSCT initiation was chosen by a random number generator (same data sets), the latency increased significantly to 584 ± 545 ms (ANOVA significance at $p < .05$ by Scheffe F test), providing further evidence that the temporal association between MESCs and MSCTs is not random.

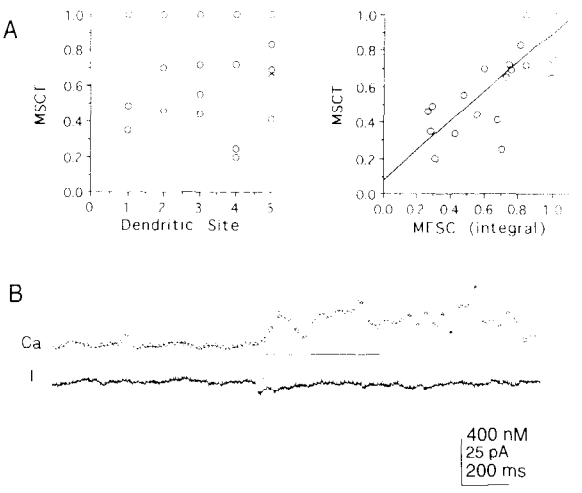

Figure 3. A Correlation between Variability in MSCTs and MESCs

(A) MSCTs and MESCs were quantitated (see [B]) for single dendritic sites that exhibited multiple MSCTs. To compare these quantities between different synapses and different cells, the MESCs and MSCTs were normalized to the maximal response measured at a particular synaptic site (the largest MSCT or MESC at a given site would be equal to 1.0). (Left) Relative MSCTs for 5 different dendritic sites during repeated MSCTs at these sites (from 3 different neurons). At site 5, 2 MSCTs had values of 0.65; to resolve them on the plot, we added 0.02 to 1 of the values. (Right) Values of relative MSCT and MESCs (during repeated events) were plotted (scattergram) for a total of 7 different dendritic sites from 4 different neurons. The correlation coefficient (R) of the aggregate data was 0.82.

(B) An example of how MSCT and MESC were measured. In this example, the traces shown are simultaneous records of $[Ca^{2+}]_i$ (Ca) and current (I) derived from a site of MSCT initiation on a dendritic shaft. The dotted line indicates the baseline (average resting value = 44 nM) of $[Ca^{2+}]_i$ measured at a 1 μm^2 dendritic region. The dashed line indicates 1 SD above resting $[Ca^{2+}]_i$, the threshold used to detect MSCTs (4 points must be above this value). To quantitate the MSCT, the first 15 data points, corresponding to 500 ms, were averaged. MESCs were quantitated by integrating their first 100 ms. The points included in these calculations are indicated by the solid line, and the amplitude of each point is measured from the baseline (dotted line).

Correlation of MESC and MSCT Amplitudes at Single Synaptic Sites

Examination of the current records as well as changes in Fura 2 fluorescence suggested that the amplitudes of MSCTs and their temporally associated MESCs vary when MSCT events are repeated at the same dendritic site. In our present study, in which we have imaged $[Ca^{2+}]_i$ with enhanced temporal resolution (as compared with our previous study; Murphy et al., 1994a), we observed that repeated MSCT events at a single synaptic site showed different peak amplitudes. For the example shown in Figure 2A, a presumed dendritic shaft synapse, MSCT peak amplitudes ranged from 200 to 570 nM. A comparison of these MSCT events with their corresponding synaptic currents (shown in Figure 2A, right) suggested that differences in MESC amplitude contribute to MSCT variability, as the larger amplitude MSCTs were associated with larger MESCs. The amplitudes of MESCs varied from ~5 pA (responses 1 and 2) to >20 pA (response 4). A comparison of the currents recorded from the cell soma (representative

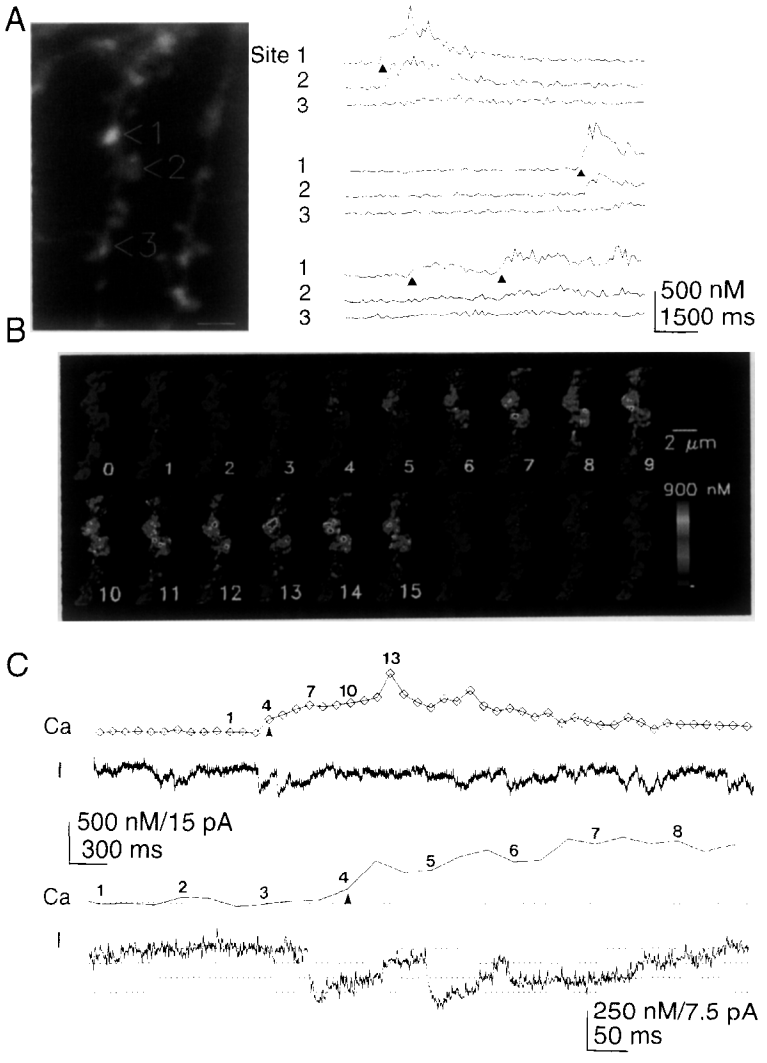

Figure 4. Images of MSCT Initiation

(A) Plots of $[Ca^{2+}]_i$ versus time, made from three different 0.8 μm^2 dendritic regions (see image) centered at the arrowheads, are shown during three different 10 s sampling epochs. The $[Ca^{2+}]_i$ records were produced by averaging over 0.1 s intervals (i.e., each point is the average of 3 consecutive images). The time point at which $[Ca^{2+}]_i$ transients were initiated is indicated by a closed arrowhead. Bar, 2 μm.

(B) Images of the initiation of the first MSCT in (A) (see top traces) at 0.1 s intervals (averages of 3 consecutive images) in the dendritic region encompassing measurement sites 1–3. Images 0–3 show the baseline preceding the transient, images 4–15 are during 1.2 s of the transient, and unlabeled images are consecutive $[Ca^{2+}]_i$ images 7 s after the transient. The edges of the $[Ca^{2+}]_i$ image were determined by setting a threshold pixel intensity that was applied to the entire image shown.

(C) (Top) Expanded record of $[Ca^{2+}]_i$ measured at site 1, with corresponding image sequences (see [B]) indicated above traces; the coincident currents are shown below (I). (Bottom) The same plot shown at higher temporal resolution. $[Ca^{2+}]_i$ measurements were made at 33 ms intervals, and the corresponding image numbers (above) and currents (below) are shown. The dotted lines (2.7 pA apart) indicate differences in MESC currents consistent with the properties of the NMDA receptor channel (in the presence of moderate dendritic filtering).

of activity from all synapses) with those corresponding to MSCTs at this synapse suggested that the output of this dendritic shaft site ranges from the amplitude seen at the weakest synapses (responses 1 and 2; see arrows) to some of the largest responses measured in this neuron (response 4). Over the same three 10 s epochs, 6 repeated MSCTs were observed at a nearby dendritic spine (Figure 2B; expanded current records are not shown). As expected for independent events, no temporal correlation was observed between the changes in amplitude of MSCTs at the spine and those of MSCTs at the shaft (Figures 2A and 2B), suggesting that factors intrinsic to each synapse, such as MESC amplitude (and not the recording procedure), affect response variability.

To address further the relationship between MSCTs and MESCs, we quantitated the responses (see Experimental Procedures and Figures 3A and 3B) at apparent high probability synapses that exhibit multiple MSCT events. As a more accurate measurement of MSCT amplitude, we averaged the first 15 data points (500 ms) of the $[Ca^{2+}]_i$ transient and used this value to compare multiple events at a single site (Figures 3A and 3B). For comparison of MSCT variability across different experiments, we normalized the MSCTs to the maximum response observed at a specific site. MSCTs observed at a single synapse and measured by this method varied by up to 5-fold (Figure 3A, left). The extent of MSCT variability was quite high, as the mean ± SD of the normalized MSCTs (excluding maximal values) was 0.52 ± 0.19 (n = 17; data from Figure 3A, right). As antagonist experiments indicated that NMDA receptor activation is required for producing MSCTs (Murphy et al., 1994a), we quantitated MESCs by integration of their first 100 ms (Figure 3B). This analysis indicated that the amplitudes of the synaptic currents were positively correlated with the MSCT amplitudes. For a total of 24 MSCT and MESC pairs from 4 different neurons, an aggregate correlation coefficient of 0.82 was calculated (see Figure 3A, right). Analysis of this population data indicated that the variability ranges of both MESCs and MSCTs at a single synapse were 4- and 5-fold, respectively (Figure 3A, right).

Images of MSCT Initiation

In analyzing sites that displayed multiple MSCTs, we generated images of $[Ca^{2+}]_i$ with reduced noise by averaging 3 consecutive video frames (off-line). These images, which

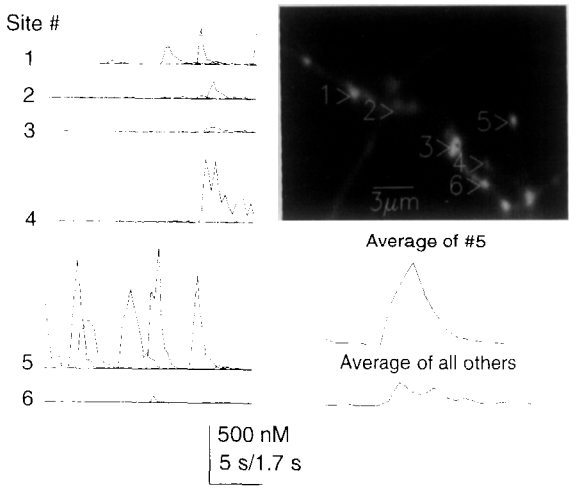

Figure 5. Variability in MSCT Amplitude between Synapses

Shown in the upper right panel is a 360 nm Fura 2 excitation image (Ca^{2+}-insensitive excitation wavelength) of an axon and a dendritic process from which the plots of $[Ca^{2+}]_i$ were made from averaged images (average of four 33 ms frames produced every 333 ms) as previously described (Murphy et al., 1994a). Plots of $[Ca^{2+}]_i$ versus time for 6 different dendritic sites of MSCT origin (left) are plotted as overlays for five different 20 s epochs. MSCTs were initiated and measured at 1.0 μm^2 sites centered at the indicated regions (arrowheads). MSCT records for site 5 (lower right) were aligned by the first rise in $[Ca^{2+}]_i$ and averaged; the average amplitude of MSCTs from site 5 was compared to that of all other synapses (8 other sites with 10 events; lower record) observed in this neuron. The average includes events from sites that are not shown. With the exception of sites 1 and 5, all sites examined exhibited only 1 MSCT event. MSCTs that were derived from the spread of $[Ca^{2+}]_i$ from adjacent synaptic sites or that occurred during the falling phase of a previous transient were excluded from analysis. All MSCTs analyzed involved at least 4 points that were 1 SD above baseline. An axon was identified by its smooth surface, small bore, perpendicular branches, and varicosities. This axon made a single, near perpendicular junction and possible contact with the dendrite within 1 μm to the left of where a single MSCT was observed at site 2. Simultaneous records of synaptic currents were not made from this neuron.

have 10 Hz temporal resolution, were used to evaluate the initiation and spread of the MSCT. A total of 4 separate MSCTs were observed at the location indicated as site 1 in Figure 4A. This initiation site was contained within an ~1 μm^2 region that had a significantly higher level of Fura 2 Ca^{2+}-insensitive fluorescence (Figure 4A, left), suggesting that it had a larger volume and was potentially a vertically projecting spine or a large dendritic varicosity. Analysis of Ca^{2+} images (the first MSCT from Figure 4A is shown in Figure 4B) and plots of $[Ca^{2+}]_i$ versus time from multiple measurement sites indicated that all 4 MSCTs were initiated from site 1 (Figure 4A; and data not shown). Measurement of $[Ca^{2+}]_i$ along the dendritic process (sites 2 and 3) indicated that larger amplitude MSCTs initiated at site 1 propagated further than the lower amplitude events (Figure 4A; compare the first 2 MSCTs with the last 2). The site of MSCT initiation and the extent of MSCT spread along the dendrite are also shown by the $[Ca^{2+}]_i$ image (Figure 4B).

To evaluate the temporal relationship between the onset of the MSCT and MESCs, we examined records of $[Ca^{2+}]_i$ from site 1 that were made from unaveraged images (33 ms time resolution; Figure 4C, bottom). These records indicated that a MESC preceded the first rise in $[Ca^{2+}]_i$ by ~50 ms. Examination of the currents that coincided with the MSCT revealed that they underwent abrupt changes in their amplitude. These changes were presumably due to the gating of a small number of NMDA receptor channels, as they approximated the single-channel conductance of the receptor (assuming some dendritic filtering). Although there was a tight temporal correlation between the onset of this MSCT and a MESC, the Ca^{2+} images indicated that $[Ca^{2+}]_i$ reached a peak ~900 ms after the initiation of the MSCT (Figure 4B, image 13). This peak did not correlate with a prominent inward current and was possibly due to intracellular release of Ca^{2+} (see Discussion). These late elevations in $[Ca^{2+}]_i$ that were not accompanied by prominent inward currents were observed at three other dendritic regions that were studied in a total of 3 different neurons.

Variability in MSCTs between Synapses

Analysis of multiple MSCTs at individual dendritic sites indicated that there is substantial event to event variability at these sites over time. To address whether differences in MSCT amplitude between synapses are within the range of variability at a single synapse, we compared the amplitude of MSCTs between synapses in an experiment in which we recorded a large number of events from 9 different dendritic sites on the same neuron (6 of the sites are shown in Figure 5). At the long-necked spine (site 5), MSCTs averaged 789 ± 251 nM (mean ± SD; n = 5), whereas the average of all other sites observed in this neuron was 237 ± 175 nM (n = 10 events at 8 sites). Statistical analysis by ANOVA indicated that the distribution of response amplitudes at spine site 5 was significantly different (significance at $p < .05$, Scheffe F test) from other sites in this neuron. Although a single synapse can exhibit considerable variability in amplitude (see Figures 2–4), these data suggest that the distribution of response amplitudes can vary between different synapses within the same neuron. Conceivably, these differences between synapses could be attributed to several factors, including the amplitude of underlying MESCs, dendritic volume or geometry, and Ca^{2+} sequestration or buffering (reviewed in Regehr and Tank, 1994).

Discussion

Correlating MSCTs and MESCs

Our previous study suggested that MSCTs are triggered by underlying MESCs (Murphy et al., 1994a). To determine their relationship directly, we made simultaneous measurements of MESCs and MSCTs. These recordings indicated that MESCs preceded the appearance of MSCTs. Since MESCs recorded at the cell soma are generated at sites throughout the dendritic tree, not just in the relatively small segments being imaged, we needed to ensure that this apparent correlation of MESCs and MSCTs was not merely a random coincidence. Analysis of the latencies between MESCs and MSCTs, as well as the ensemble average of current records associated with MSCTs (see

Figure 1B), confirmed that this correlation was not spurious. However, it is important to emphasize that, even though analysis of group data demonstrates that MSCTs are associated with MESCs, it may not be possible to assign an MESC to each MSCT. At some dendritic sites, in particular at spines and very fine dendrites (e.g., the spine in Figure 2C), small $[Ca^{2+}]_i$ transients did not always correlate with well-defined MESCs (i.e., with rapid rise time and relatively large amplitude), thus precluding unequivocal detection of the currents triggering these MSCTs. As the small volume of these dendritic compartments would be expected to amplify the $[Ca^{2+}]_i$ transient, some currents associated with events as small the opening of a single NMDA receptor channel may go undetected owing to the effects of dendritic filtering (Spruston et al., 1994).

A Comparison between MESC and MSCT Frequency

Measurement of MSCT frequency indicated that synapses can exhibit MESCs at frequencies in the range of 0.1 Hz (see Figures 2, 4, and 5) (Murphy et al., 1994a). A comparison of the frequency of MESCs per synapse to that of MESCs per neuron (which ranged from 1 to 5 Hz) indicated that as few as 10–50 synapses could account for most of the MESCs recorded. To address this issue further, we used presynaptic markers and estimated that our preparation has in excess of 1000 synapses per neuron (Murphy et al., 1994a). By imaging a single dendritic region for a relatively long period of time (2–3 min), we estimated, based on distinct MSCT initiation sites, that the number of functional excitatory synapses is at least 100–200 per neuron (T. H. M. et al., unpublished data). Thus, differences in the probability of spontaneous activity between synapses may account for the apparent disparity between the number of synapses identified and the relatively low frequency of MESCs recorded. In support of this hypothesis, we have shown previously that some synaptic sites exhibit multiple MSCTs, while others exhibit lower frequencies or are silent over the 1–2 min of total imaging during a single experiment (Murphy et al., 1994a). Statistical analysis indicated that some sites have a significantly higher probability of activity than the general population. Consistent with our findings, two separate laboratories that measured the use-dependent block of the evoked excitatory postsynaptic current by MK-801 estimated that the probability of evoked release varies widely between different synaptic terminals (Hessler et al., 1993; Rosenmund et al., 1993). Furthermore, using Ca^{2+} imaging, Malinow et al. (1994) reported that Ca^{2+} transients with characteristics similar to those of MSCTs can be evoked by presynaptic stimulation and used to locate high and low probability synapses in hippocampal slices.

Glutamate Receptor Types and MSCTs

Glutamate mediates fast excitatory synaptic currents in these cultures (Murphy et al., 1992). MESCs produced by glutamate receptors have different kinetic components attributed to NMDA and non-NMDA receptor types (Bekkers and Stevens, 1989; Hestrin et al., 1990; Silver et al., 1992). Detection of kinetic components attributed to both receptor types in a single MESC has provided evidence that non-NMDA- and NMDA-type glutamate receptors are colocalized at single synapses (Bekkers and Stevens, 1989). MESCs recorded from our preparation of cultured cortical neurons often have a relatively prominent, slow kinetic component (see Figure 1B; Figure 3B; Figure 4C), although MESCs with biphasic kinetics are observed in Figure 1C. As seen in previous studies (Bekkers and Stevens, 1989; Silver et al., 1992), in the presence of the NMDA receptor antagonist D,L-APV (80 μM), we observed only MESCs with relatively rapid kinetics (data not shown), suggesting that the slow component is mediated by NMDA receptors. In this study, as previously reported (Murphy et al., 1994a), we observed a complete absence of MSCTs in the presence of D,L-APV (80 μM). These findings suggest that MSCTs are triggered by the NMDA receptor component of MESCs. In contrast to the effects of NMDA receptor antagonists, MSCTs were still observed in the presence of the non-NMDA-type glutamate receptor antagonist 6-cyano-7-dinitroquinoxaline (CNQX; 5–10 μM; n = 2 neurons). However, we cannot, from these preliminary experiments, exclude the possibility that blockade of non-NMDA receptors may reduce the amplitude or frequency of MSCTs. In addition, although the voltage-clamp recording mode was used, we cannot rule out a potential involvement of voltage-gated Ca^{2+} channels (Jaffe et al., 1994; Markram and Sakmann, 1994) in MSCTs, as it is possible that voltage-clamp control may be lost locally owing to the complex dendritic geometry. Further evidence for a role of NMDA receptors was provided by the complete blockade of MSCTs when $[MgCl_2]_o$ was raised from nominally free to 1 mM (at resting membrane potential; n = 2 neurons). The effect of elevated Mg^{2+} was reversed when Mg^{2+}-free solution was washed in. Examination of the kinetics of the MESCs (which correlate temporally with MSCTs) indicated that different synaptic sites may vary in their complement of NMDA- and non-NMDA-type glutamate receptors (data not shown). However, owing to the large amount of event to event variability observed in MESCs (at a single synapse; see Figures 1–4) and the relative paucity of non-NMDA-type currents, much longer recording periods than those used in this study would be needed to address this issue rigorously. Therefore, our results are applicable only to variability of the NMDA receptor component of MESCs both between synapses and within a single synaptic site.

Stochastic Properties of NMDA Receptor Channels and Variability in Synaptic Output

Our study, which utilizes measurements of both postsynaptic $[Ca^{2+}]_i$ and synaptic currents, demonstrates that a single synapse can have variable output and supports previous studies (Andersen et al., 1990; Bekkers et al., 1990; Raastad et al., 1992; Gulyas et al., 1993). However, our results would appear to contradict studies that suggest a saturating concentration of glutamate is achieved following the release of a single transmitter quantum (Clements et al., 1992; Tang et al., 1994; Tong and Jahr, 1994). If a single transmitter quantum saturates postsynaptic glutamate receptors, increases in synaptic vesicle content or number would not be expected to affect postsynaptic out-

put. On the other hand, postsynaptic factors could explain the variability in synaptic response, such as the stochastic properties associated with small numbers of NMDA receptor channels (Faber et al., 1992) or modulation of receptor function (reviewed in Raymond et al., 1993). Consistent with a stochastic mechanism, as few as four NMDA receptor channels are thought to mediate the NMDA receptor component of a MESC (Bekkers and Stevens, 1989; Robinson et al., 1991; Silver et al., 1992). As these receptors are Ca^{2+} permeable, these properties would account for the observed variability in MSCT amplitudes. In some experiments in which we have correlated MSCTs with MESCs at sites very close to the cell body (within 50 μm) and used cesium in the pipette solution, we have observed changes in the MESC currents consistent with the involvement of as few as three or four NMDA receptor channels in mediating the onset of a MSCT (see Figure 4C). These abrupt alterations in current approximated the amplitude expected for 40–50 pS NMDA receptor channels observed in MESCs (Robinson et al., 1991; Silver et al., 1992). Thus, when MESCs occur at fine dendritic processes and spines, stochastic variability (i.e., whether one, two, or three NMDA receptor channels are activated) could produce particularly large differences in $[Ca^{2+}]_i$, owing to the relatively small volume of the postsynaptic element.

Multiquantal Responses and Variability in Postsynaptic Output

Another possible explanation for variable synaptic output is that MESCs (within these cultures) are not always produced by a single transmitter quantum. If there were mechanisms to prevent receptor saturation, multiquantal activity would be a means of enhancing postsynaptic output. Consistent with this proposal, previous studies have described multiquantal responses occurring at neuronal synapses (Korn et al., 1993; Trussell et al., 1993; Tong and Jahr, 1994) during both evoked and spontaneous synaptic responses. Multiquantal responses are thought to arise from the cooperative release of more than one transmitter quantum from a single presynaptic terminal. Conceivably, changes in the number or frequency of quanta released could result in synaptic currents and Ca^{2+} transients of varying amplitude. Multiquantal activity can be observed under basal conditions, although it is particularly apparent during manipulations that promote neurotransmitter release, such as elevated $[Ca^{2+}]_o$ or paired-pulse facilitation (Korn et al., 1993; Trussell et al., 1993; Tong and Jahr, 1994). Therefore, the elevated $[Ca^{2+}]_o$ we have used to enhance postsynaptic MSCTs might promote multiquantal responses.

Though factors intrinsic to a particular synapse could govern the variability we have observed in synaptic output, it is also possible that more than one synapse (or release site) exists at these dendritic sites. Multiple synapses could occur if axons and dendrites ran parallel to each other, permitting multiple closely spaced contacts. However, the intersections between Fura 2–injected axons and dendrites did not display parallel appositions, which suggested only one contact point (n = 5 neurons; see Figure 5). Furthermore, we did not detect any shift (greater than ~1.0 μm) in the location at which the Ca^{2+} transient was first initiated during the repeated events seen at the dendritic shaft sites. In addition, variation in MSCT amplitude was observed at the tips of long-necked spines (~5 μm; e.g., see Figure 2B and Figure 5), which, given the low synaptic density of these cultures (Murphy et al., 1994a; compared with in vivo), would not be expected to have more than one excitatory synapse (reviewed in Harris and Kater, 1994). However, the presumed presence of only one synapse at these sites does not preclude the possibility that there is more than one release site contributing to the output variability observed.

Single MESCs Do Not Invariably Result in Saturating Levels of $[Ca^{2+}]_i$

Based on the modeling studies of Zador et al. (1990), single MESCs occurring at spine heads (~1 μm in diameter) are expected to produce elevations in $[Ca^{2+}]_i$ in the range of 10 μM. In a preliminary computer model (data not shown) that incorporates features of our experimental conditions, such as $[Ca^{2+}]_o$, $[Mg^{2+}]_o$, and Fura 2 concentration, as well as cellular buffers and pumps (using values that approximated those in Zador et al., 1990), we estimated that the NMDA receptor component of a single MESC that involves three channels would produce a spatially averaged transient in excess of 50 μM. This high $[Ca^{2+}]_i$ value was calculated despite the inclusion of relatively high concentrations of Ca^{2+} pumps and Fura 2 in the model. This $[Ca^{2+}]$ would be expected to saturate the Fura 2 Ca^{2+} probe (K_D = 200 nM) as well as most physiologically relevant postsynaptic targets, such as calmodulin (Teo and Wang, 1973). In contrast to this prediction, we always observed that spatially averaged $[Ca^{2+}]_i$ transients were <1.3 μM in spine heads (measured over a 1 μm^2 area). Although there is likely to be some error associated with the Fura 2 calibration, a large amount of variability in $[Ca^{2+}]_i$ transient amplitude (MSCTs) was apparent at a single synaptic site (see Figures 2–5) during repeated events. This variability would not be expected if the rise in $[Ca^{2+}]_i$ associated with a single MESC always resulted in saturation of the Fura 2 probe (i.e., $[Ca^{2+}]_i$ greater than 2 μM; 10× the K_D). The ability of small dendritic compartments such as spines to exhibit Ca^{2+} responses within the range of physiological Ca^{2+} affinities permits a graded postsynaptic biochemical response that is related to the frequency or amplitude of synaptic stimulation (Murphy et al., 1994b). Consistent with this idea, Regehr and Tank (1992) and Petrozzino et al. (1993; Soc. Neurosci., abstract) used low affinity $[Ca^{2+}]_i$ probes to show that spatially averaged $[Ca^{2+}]_i$ transients triggered by high frequency synaptic stimulation (that presumably results in a summation of MSCTs) can be in excess of 10 μM.

MESCs Trigger Delayed Elevations in $[Ca^{2+}]_i$

Simultaneous $[Ca^{2+}]_i$ imaging and measurement of synaptic currents indicated a correlation between the amplitudes of MSCTs and MESCs. However, in many cases (see Figures 1B and 1C; Figure 2A; Figure 3B; Figures 4B and 4C) neurons exhibited spike-like changes in $[Ca^{2+}]_i$ during the plateau or falling phase of the $[Ca^{2+}]_i$ transient that did

not correlate with substantial synaptic currents. Although these spikes did not correlate with the peak of MESC activity, we cannot exclude that they were triggered by the opening of a single NMDA receptor channel. Interestingly, in many cases these spikes represented the peak amplitude of the MSCT (see above examples). The spikes did not appear to be associated with random noise, as they were observed in multiple sequential video frames, were well separated from the upstroke of the MSCT, and were initiated at synaptic sites in regions that exhibited a relatively high fluorescence signal to noise ratio (see Figures 4A and 4B). It is conceivable that these changes in $[Ca^{2+}]_i$ are produced by the release of Ca^{2+} from internal stores (Tsien and Tsien, 1990; Friel and Tsien, 1992). Increases in $[Ca^{2+}]_i$ that persist after the decay of a Ca^{2+} current that triggers them have been described in neurons (Hernández-Cruz et al., 1990). Furthermore, Alford et al. (1993) observed that conditions which attenuate release of Ca^{2+} from intracellular stores suppress the peak amplitude of synaptically evoked $[Ca^{2+}]_i$ transients recorded in hippocampal slices. These authors also observed oscillatory behavior during the falling phase of synaptically evoked Ca^{2+} transients.

Synapses with a High Frequency of MSCTs Reflect Increased Transmitter Release

In our initial study (Murphy et al., 1994a), we were unable to determine whether the repeated appearance of MSCTs at a single dendritic site was due to increased transmitter release or increased postsynaptic sensitivity. Although MSCTs occurred at a significantly higher frequency at these sites, suggesting increased transmitter release and a presynaptic mechanism, we were concerned that the method was not sufficiently sensitive to resolve low amplitude MSCTs. For example, if all synapses had the same frequency of MSCTs but those with low amplitude events went undetected, the synapses with large amplitude events might be mistakenly labeled (by their apparent high frequency) as sites with presynaptic modifications that led to high release probabilities. Measurements of MESC and MSCT amplitude at single postsynaptic sites performed in the present study indicate that MSCTs can be associated with the smallest MESCs recorded from a neuron. This observation indicates that the sensitivity of our imaging technique is not limiting and that dendritic sites with a high frequency of MSCTs are likely to have a higher probability of transmitter release.

Conclusion

By simultaneously measuring the amplitudes of MESCs and their associated Ca^{2+} transients, we have shown that central synapses exhibit variable output. The ability of individual synapses to vary their output permits a large repertoire of graded synaptic responses. Calcium transients of graded amplitude may provide a means of engaging specific biochemical pathways at different levels of $[Ca^{2+}]_i$. These pathways may trigger distinct forms of neuronal plasticity such as long-term potentiation and depression (Dudek and Bear, 1992; Mulkey and Malenka, 1992). Our results suggest that, even though quantal release is considered to be a unitary form of synaptic transmission, the postsynaptic response to this stimulus is highly plastic and will likely depend on dynamic changes in receptor properties and structural features of the local dendritic environment.

Experimental Procedures

Cortical neurons and glia were dissociated from 17–18 day gestation rat fetuses, placed in culture, and allowed to mature for 17–26 days in vitro as previously described (Murphy and Baraban, 1990), with the exception that the plating medium L-cystine concentration was supplemented to 300 μM. For Fura 2 loading (Grynkiewicz et al., 1985), neurons were impaled with 40–60 MΩ microelectrodes filled (tip only) with 10 mM Fura 2 (K^+ salt; Molecular Probes) in 200 mM KCl (Murphy et al., 1994b). In some experiments (such as those in Figure 4 and Figure 5), neurons were loaded under the whole-cell recording mode using patch-clamp pipettes (~10–12 MΩ; containing 5–10 mM Fura 2, 150 mM KCl, and 10 mM HEPES). After the neurons were loaded (~10 min for microelectrodes and usually <2 min for patch-clamp pipettes), the electrodes were removed and the cells were allowed to recover in the presence of TTX for about 2–3 hr. Ratiometric Fura 2 imaging was performed at room temperature as described previously (Blatter and Wier, 1990). Calibration parameters for Fura 2 were determined in vivo by intracellular perfusion of neurons using patch-clamp pipettes containing 300 μM Fura 2 salt and a solution with either no added Ca^{2+} (plus 20 mM EGTA) or 10 mM Ca^{2+} and no EGTA, over a 10–30 min period during which images of both fine dendritic processes and the cell soma were taken. This calibration indicated that 300 μM Fura 2 approximates the amount microinjected. Plots of $[Ca^{2+}]_i$ versus time were produced from either single video frames (30 frames per second) or 3–4 frame averages (Murphy et al., 1994a) as indicated. The following extracellular solution (which lacked magnesium) was used to isolate MESCs: 137 mM NaCl, 5.0 mM KCl, 5.0 mM $CaCl_2$, 0.34 mM $Na_2HPO_4(H_2O)_7$, 10 mM Na^+–HEPES, 1 mM $NaHCO_3$, 0.01–0.1 mM picrotoxin, 0.001 mM TTX, 22 mM glucose (pH 7.4; 340 mOsm). Cells were switched to this solution at least 10 min before MSCT imaging. Prior to all experiments, neurons were synaptically stimulated by picrotoxin-induced bursting (in the absence of TTX; Murphy et al., 1992) to increase the number of synapses with repeated MSCT events (Murphy et al., 1994a).

For simultaneous measurements of synaptic currents and MSCTs, we used a Nikon or a Zeiss 100×, 1.3 NA objective and positioned the cell body of a Fura 2–filled neuron at the edge of the microscopic field so that fine dendritic processes (which were usually within 80 μm of the soma) were visible in the video field. Typically, we chose neurons with small and relatively uncomplicated dendritic arbors, since we could image a larger percentage of these neurons and they tended to have a lower frequency of MESCs, which reduces spurious correlations between MESCs and MCSTs. Small bore (<3 μm in diameter) dendrites that made a direct connection with the cell body were usually imaged. Prior to all electrophysiological recordings, we examined several different dendritic regions to select one with a high frequency of MSCTs.

The perforated patch-clamp recording method (Horn and Marty, 1988) was used to record spontaneous synaptic currents at a holding potential of −80 mV (cells previously injected with Fura 2). This method has several advantages over the whole-cell method: cellular $[Ca^{2+}]_i$ buffering and energy stores are intact, Fura 2 concentration is constant throughout the experiment, and cell viability can be checked before recording by assessing resting $[Ca^{2+}]_i$ levels. For perforated patch-clamp recordings, 6–9 MΩ patch pipettes were filled (tip only) with nystatin-free solution (120 mM $KMeSO_4$, 10 mM HEPES, 25 mM KCl, 10 mM $MgCl_2$; pH 7.4), and the remainder of the electrodes were filled with the same solution containing nystatin (130–170 μg/ml; diluted from a 50 mg/ml dimethylsulfoxide stock). In a few experiments, 25 mM CsCl (see Figure 4) was substituted for KCl. After a 15–20 min period in which nystatin channels inserted and produced a reduction in series resistance to a stable value (which ranged from 10 to 35 MΩ), simultaneous recordings of membrane current and $[Ca^{2+}]_i$ images were made during 10 s sampling epochs. In none of the experiments analyzed was there a substantial loss of the Fura 2 probe indicative of membrane rupture and a loss of the perforated patch-clamp recording

mode. In a few experiments (see Figure 1C), the whole-cell recording configuration was used, in which cells were dialyzed with an internal solution containing 0.5 mM Fura 2 K^+ salt, 142 mM $CsMeSO_4$, 5 mM Mg^+–ATP, and 10 mM HEPES (pH 7.2, adjusted with HCl and NaOH). Currents recorded with both methods were pooled for the analysis in Figure 1B. Because of potential for intracellular dialysis and changes in Fura 2 concentration in the whole-cell configuration, we did not use $[Ca^{2+}]_i$ transients recorded in the whole-cell mode for the evaluation of MSCT amplitude variability in Figures 2–4. Currents were digitized at 1.4–2 kHz and low-pass filtered at 0.5–1 kHz. A fiber-optically coupled, intensified CCD camera with a Gen III intensifier tube was used for all experiments (Stanford Photonics, Palo Alto, CA). For each 10 s epoch, 300 images were collected and stored digitally using an Imaging Technology Series 151 image processor and an Applied Memory Technology real time disk recorder (for most cells, only six epochs could be collected). In some experiments, an Epix 4M12–64 MB frame grabber board was used. Images and the recorded currents were analyzed together on an IBM RISC 6000 workstation or a Pentium 90 MHz microcomputer using custom routines written in the program IDL (Research Systems, Inc.). To synchronize current records with the images, a pulse based on when current records were initiated was added to the video signal.

In cases in which the amplitudes of repeated events were quantitatively compared at a single dendritic site (see Figure 2; Figure 3), we included only current records made within a 6 min period over which input resistance and the average amplitude of MESCs (representative of activity from all synapses) did not vary by more than 20%. To correlate MSCTs and MESCs temporally, it was important to determine precisely the time and site of MSCT initiation. The initiation site had the earliest rise in $[Ca^{2+}]_i$ and usually the greatest rate of rise. In almost all cases, the dendritic location of MSCT initiation (a putative synaptic site) had a structurally identifiable feature, such as a varicosity or a spine. In some cases, spines projecting into the Z axis may appear as a varicosity or a bright spot. Ca^{2+} transients were considered MSCTs if at least 4 consecutive measurements from 33 ms video frames were more than 1 SD above the baseline noise level (measured from a 0.8–2.0 μm^2 area). The initiation time of a MSCT was defined as the first measurement (33 ms video frame of unfiltered data) that was more than 1 SD above the baseline noise. The end of a MSCT was defined as a return to within 1 SD of baseline for at least 4 measurements. In some cases, the time of MSCT initiation was determined from the analysis of raw 380 nm Fura 2 excitation images (instead of $[Ca^{2+}]_i$ images; e.g., see Figure 1C). By defining a MSCT by its persistence above baseline for at least 4 video frames, we were able to exclude from our analysis potentially small and brief changes in $[Ca^{2+}]_i$ due to spontaneous unitary Ca^{2+} release events or "sparks," which in cardiac cells have a ~10 ms rise time and a 20 ms decay time (Cheng et al., 1993). For the calculation of correlation coefficients for MESC and MSCT amplitudes at single dendritic sites, we excluded Ca^{2+} transients that occurred during the decay phase of a previous transient. Since the synaptic currents leading to MSCTs have slow components, we used charge transfer measurements (the first 100 ms of a MESC current) for correlation with MSCT amplitude. As records of $[Ca^{2+}]_i$ at 30 Hz resolution often had multiple peaks, we averaged the first 15 frames (500 ms) of the Ca^{2+} transient for the correlation with currents.

Acknowledgments

All correspondence should be addressed to T. H. M. We would like to thank Lynn Raymond, Paul Mackenzie, Masashi Umemiya, and David Linden for helpful comments on this manuscript, and Hose Lopez-Lopez Ramon and Phil Shacklock (University of Maryland) for assistance with imaging software. This work was supported by United States Public Health Service grants MH-00926 and DA-00266 to J. M. B., grants from the American Heart Association and the USPHS to W. G. W., and grants from the Medical Research Council of Canada and the British Columbia Health Research Fund to T. H. M. T. H. M. is an Alfred P. Sloan and Medical Research Council Scholar.

The costs of publication of this article were defrayed in part by the payment of page charges. This article must therefore be hereby marked *"advertisement"* in accordance with 18 USC Section 1734 solely to indicate this fact.

Received June 16, 1994; revised April 12, 1995.

References

Alford, S., Frenguelli, B. G., Schofield, J. G., and Collingridge, G. L. (1993). Characterization of Ca^{2+} signals induced in hippocampal CA1 neurons by the synaptic activation of NMDA receptors. J. Physiol. *469*, 693–716.

Amaral, D. G., Ishizuka, N., and Claiborne, B. (1990). Neurons, numbers and the hippocampal network. Prog. Brain Res. *83*, 1–11.

Andersen, P., Raastad, M., and Storm, J. F. (1990). Excitatory synaptic integration in hippocampal pyramids and dentate granule cells. Cold Spring Harbor Symp. Quant. Biol. *87*, 81–86.

Bekkers, J. M., and Stevens, C. F. (1989). NMDA and non-NMDA receptors are co-localized at individual excitatory synapses in cultured rat hippocampus. Nature *341*, 230–233.

Bekkers, J. M., Richerson, G. B., and Stevens, C. F. (1990). Origin of variability in quantal size in cultured hippocampal neurons and hippocampal slices. Proc. Natl. Acad. Sci. USA *87*, 5359–5362.

Blatter, L. A., and Wier, W. G. (1990). Agonist-induced $[Ca^{2+}]_i$ waves and Ca(2+)-induced Ca^{2+} release in mammalian vascular smooth muscle cells. Am. J. Physiol. *263*, 576–586.

Carmignoto, G., and Vicini, S. (1992). Activity-dependent decrease in NMDA receptor responses during development of visual cortex. Science *258*, 1007–1011.

Cheng, H., Lederer, W. J., and Cannell, M. B. (1993). Calcium sparks: elementary events underlying excitation contraction coupling in heart muscle. Science *262*, 740–744.

Clements, J. D., Lester, R. A. J., Tong, G., Jahr, C. E., and Westbrook, G. L. (1992). The time course of glutamate in the synaptic cleft. Science *258*, 1498–1501.

Dudek, S. M., and Bear, M. F. (1992). Homosynaptic long-term depression in area CA1 of hippocampus and effects of N-methyl-D-aspartate receptor blockade. Proc. Natl. Acad. Sci. USA *89*, 4363–4367.

Faber, D. S., Young, W. S., Legendre, P., and Korn, H. (1992). Intrinsic quantal variability due to stochastic properties of receptor–transmitter interactions. Science *258*, 1494–1498.

Friel, D. D., and Tsien, R. W. (1992). Phase-dependent contributions from Ca^{2+} entry and Ca^{2+} release to caffeine-induced $[Ca^{2+}]_i$ oscillations in bullfrog sympathetic neurons. Neuron *8*, 1109–1125.

Gulyas, A. I., Miles, R., Sik, A., Toth, K., Tamamaki, N., and Freund, T. F. (1993). Hippocampal pyramidal cells excite inhibitory neurons through a single release site. Nature *366*, 683–687.

Grynkiewicz, G., Poenie, M., and Tsien, R. Y. (1985). A new generation of calcium indicators with greatly improved fluorescence properties. J. Biol. Chem. *260*, 3440–3450.

Harris, K. M., and Kater, S. B. (1994). Dendritic spines: cellular specializations imparting both stability and flexibility to synaptic function. Annu. Rev. Neurosci. *17*, 341–371.

Hernández-Cruz, A., Sala, F., and Adams, P. R. (1990). Subcellular calcium transients visualized by confocal microscopy in a voltage-clamped vertebrate neuron. Science *247*, 858–862.

Hessler, N. A., Shirke, A. M., and Malinow, R. (1993). The probability of transmitter release at a mammalian central synapse. Nature *366*, 569–572.

Hestrin, S. (1992). Developmental regulation of NMDA receptor-mediated synaptic currents at a central synapse. Nature *357*, 686–689.

Hestrin, S., Perkel, D. J., Sah, P., Manabe, T., Renner, P., and Nicoll, R. A. (1990). Physiological properties of excitatory synaptic transmission in the central nervous system. Cold Spring Harbor Symp. Quant. Biol. *87*, 000–000.

Horn, R., and Marty, A. (1988). Muscarinic activation of ionic currents measured by a new whole-cell recording method. J. Gen. Physiology *92*, 145–159.

Jaffe, D. B., Fisher, S. A., and Brown, T. H. (1994). Confocal laser scanning microscopy reveals voltage-gated calcium signals within hippocampal dendritic spines. J. Neurobiol. *25*, 220–233.

Koch, C., and Zador, A. (1993). The function of dendritic spines: devices subserving biochemical rather than electrical compartmentalization. J. Neurosci. *13*, 413–422.

Korn, H., Bausela, F., Charpier, S., and Faber, D. S. (1993). Synaptic noise multiquantal release at dendritic synapses. J. Neurophysiol. *70*, 1249–1254.

Lisman, J. E., and Harris, K. M. (1993). Quantal analysis and synaptic anatomy—integrating two views of hippocampal plasticity. Trends Neurosci. *16*, 141–147.

Malinow, R., Otmakhov, N., Blum, K. I., and Lisman, J. (1994). Visualizing hippocampal synaptic function by optical detection of Ca^{2+} entry through the NMDA channel. Proc. Natl. Acad. Sci. USA *91*, 8170–8174.

Markram, H., and Sakmann, B. (1994). Calcium transients in dendrites of neocortical neurons evoked by single subthreshold excitatory postsynaptic potentials via low-threshold-voltage activated calcium channels. Proc. Natl. Acad. Sci. USA *91*, 5207–5211.

Miyakawa, H., Ross, W. N., Jaffe, D., Callaway, J. C., Lasser-Ross, N., Lisman, J. E., and Johnston, D. (1992). Synaptically activated increases in Ca^{2+} concentration in hippocampal CA1 pyramidal cells are primarily due to voltage-gated Ca^{2+} channels. Neuron *9*, 1163–1173.

Mulkey, R. M., and Malenka, R. C. (1992). Mechanisms underlying induction of homosynaptic long-term depression in area CA1 of the hippocampus. Neuron *9*, 967–975.

Muller, W., and Connor, J. A. (1991). Dendritic spines as individual neuronal compartments for synaptic Ca^{2+} responses. Nature *354*, 73–76.

Murphy, T. H., and Baraban, J. M. (1990). Glutamate toxicity in immature cortical neurons precedes development of glutamate receptor currents. Dev. Brain Res. *57*, 146–150.

Murphy, T. H., Blatter, L. A., Wier, W. G., and Baraban, J. M. (1992). Spontaneous synchronous calcium transients in cultured cortical neurons. J. Neurosci. *12*, 4834–4845.

Murphy, T. H., Baraban, J. M., Wier, W. G., and Blatter, L. A. (1994a). Visualization of quantal synaptic transmission by dendritic calcium imaging. Science *263*, 529–532.

Murphy, T. H., Blatter, L. A., Bhat, R. V., Fiore, R. S., Wier, W. G., and Baraban, J. M. (1994b). Differential regulation of calcium/calmodulin-dependent protein kinase II and p42 MAP kinase activity by synaptic transmission. J. Neurosci. *14*, 1320–1331.

Perkel, D. J., Petrozzino, J. J., Nicoll, R. A., and Connor, J. A. (1993). The role of Ca^{2+} entry via synaptically activated NMDA receptors in the induction of long-term potentiation. Neuron *11*, 817–823.

Raastad, M., Storm, J. F., and Andersen, P. (1992). Putative single quantum and single fibre excitatory postsynaptic currents show similar amplitude range and variability in rat hippocampal slices. Eur. J. Neurosci. *4*, 113–117.

Raymond, L. A., Blackstone, C. D., and Huganir, R. L. (1993). Phosphorylation of amino acid receptors in synaptic plasticity. Trends Neurosci. *16*, 147–153.

Regehr, W. G., and Tank, D. W. (1990). Postsynaptic NMDA receptor-mediated calcium accumulation in hippocampal CA1 pyramidal cell dendrites. Nature *345*, 807–810.

Regehr, W. G., and Tank, D. W. (1992). Calcium concentration dynamics produced by synaptic activation of CA1 hippocampal pyramidal cells. J. Neurosci. *12*, 4202–4223.

Regehr, W. G., and Tank, D. W. (1994). Dendritic calcium dynamics. Curr. Opin. Neurobiol. *4*, 373–382.

Robinson, H. P., Sahara, Y., and Kawai, N. (1991). Nonstationary fluctuation analysis and direct resolution of single channel currents at postsynaptic sites. Biophys. J. *59*, 295–304.

Rosenmund, C., Clements, J. D., and Westbrook, G. L. (1993). Nonuniform probability of glutamate release at a hippocampal synapse. Science *262*, 754–757.

Silver, R. A., Traynelis, S. F., and Cull-Candy, S. G. (1992). Rapid-time-course miniature and evoked excitatory currents at cerebellar synapses *in situ*. Nature *355*, 163–166.

Spruston, N., Jaffe, D. B., and Johnston, D. (1994). Dendritic attenuation of synaptic potentials and currents: the role of passive membrane properties. Trends Neurosci. *17*, 161–166.

Stevens, C. F. (1993). Quantal release of neurotransmitter and long-term potentiation. Cell *72*/Neuron *10* (Suppl.), 55–63.

Tang, C.-M., Margulis, M., Shi, Q.-Y., and Fielding, A. (1994). Saturation of postsynaptic glutamate receptors after quantal release of transmitter. Neuron *13*, 1385–1393.

Teo, T. S., and Wang, J. H. (1973). Mechanism of activation of a cyclic adenosine 3′-5′-monophosphate phosphodiesterase from bovine heart by calcium ions. J. Biol. Chem. *248*, 5950–5955.

Trussell, L. O., Zhang, S., and Raman, I. M. (1993). Desensitization of AMPA receptors upon multiquantal neurotransmitter release. Neuron *10*, 1185–1196.

Tsien, R. W., and Tsien, R. Y. (1990). Calcium channels, stores, and oscillations. Annu. Rev. Cell Biol. *6*, 715–760.

Tong, G., and Jahr, C. E. (1994). Multivesicular release from excitatory synapses of cultured hippocampal neurons. Neuron *12*, 51–59.

Zador, A., Koch, C., and Brown, T. H. (1990). Biophysical model of a Hebbian synapse. Proc. Natl. Acad. Sci. USA *87*, 6718–6722.